

The Role of Markstein Number on the Turbulent Flame Speed and Its Scaling

Swetaprovo Chaudhuri*, Fujia Wu and Chung K. Law

Department of Mechanical and Aerospace Engineering,

Princeton University, Princeton, NJ 08544-5263, USA

Abstract: *In this paper we clarify the role of the Markstein Number (Mk) on the turbulent flame speed and its scaling, from experimental measurements on constant-pressure expanding turbulent flames. Turbulent flame speed data are presented for methane, ethylene and n-butane-air premixed flames with negative and positive Mk , propagating in nearly homogenous isotropic turbulence in a dual-chamber, fan-stirred vessel. The cold flow is characterized by high-speed particle image velocimetry, while the flame propagation rate is obtained by tracking high-speed Schlieren images. For all fuel-air mixtures of C_1 - C_4 hydrocarbons presented in this work, the normalized turbulent flame speed data follows the recent theoretical [Chaudhuri, Akkerman and Law, *Physical Review E*, 84, (2011) 026322] and experimental [Chaudhuri, Wu, Zhu and Law, *Physical Review Letters*, 108, (2012), 044503] $Re_{T,f}^{0.5}$ scaling, where the average radius is the length scale and thermal diffusivity is the transport property. For a constant $Re_{T,f}$, it is experimentally observed that the normalized turbulent flame speed decreases with increasing Mk . Such an observation could be explained as a cumulative effect of flame curvatures controlled by Mk , from the largest to the smallest scales i.e. from the mean flame radius to the flame thickness with the smaller scales dominating due to their inherent large curvatures. Recent theoretical results qualitatively predict and explain such an observation as well.*

Keywords: *Turbulent Flame Speed, Markstein Number, Expanding Flames*

1. Introduction: The turbulent flame speed is a topic of sustained interest in combustion and turbulence research, as evidenced by the large volume of analytical [1-8], experimental [9-15], computational [16-17] and review literature [18-22] that has emerged. Its practical relevance can be readily appreciated by recognizing that, being a measure of the flame surface density, turbulent flame speed can be correlated to the volumetric heat release rate in a turbulent reacting flow. Fundamentally the problem is of considerable complexity, which is further compounded by the disagreement between theories as well as the high degree of scatter of the experimental turbulent flame speeds and their sensitivity on the geometry and type of the burner used in the investigation [19]. Consequently, while understanding of the laminar flame speed is at such an advanced stage that it is now routinely used for validating reaction mechanisms, the hindrances just mentioned have prevented utilization of turbulent flame speed as a meaningful physical quantity for prediction and validation of turbulent reacting flow simulations.

Fundamentally, under the long-held assumption that the turbulent flame speed is a meaningful physical quantity, there is the interest to seek a unified scaling description, at least under some special flow conditions such as those in homogenous isotropic turbulence. The most obvious choice of the flame parameters for such a scaling in the large Damköhler number limit would be the planar laminar flame speed S_L and the corresponding laminar flame thickness δ_L . The problem of turbulent flame propagation can then be considered as a geometric one in which the effect of turbulence is to wrinkle the flame at a multitude of length scales without perturbing the inner flame structure. Such a problem was recently considered in [24] for unity Lewis number (Le) and positive Markstein Number (Mk) statistically planar flame propagating in homogenous isotropic turbulence. The turbulent flame speed normalized by the corresponding laminar flame speed for large turbulent Reynolds number (Re_T) was given to the leading order by

$$S_T / S_L \sim [(u_{rms} / S_L)(\lambda_I / \delta_L)]^{1/2} \quad (1)$$

where u_{rms} is the root mean square of velocity fluctuations and λ_I is the velocity integral length scale which was assumed to be the hydrodynamic length scale of the flame.

Non-equidiffusive transport in flames due to non-unity Lewis number (Le) results in variations of Mk . Furthermore, the Lewis number can also flip around unity for lean and rich

mixtures, as well as for hydrocarbon fuels that are lighter and heavier than the largely diffusively neutral C_2 species. Hence quantification and fundamental understanding of Mk effects on the turbulent flame speed is a primary necessity for arriving at a unified scaling of turbulent flame speed, valid for any arbitrary fuel over a large range of equivalence ratios. The negative Mk flames are particularly interesting as such flames are cellularly unstable through the thermo-diffusive instability. Consequently, while positive Mk assists in dissipating flame surface fluctuations, negative Mk promotes amplification of perturbations at wavenumber smaller than the corresponding flame thickness. Hence, Mk is expected to have a strong influence on the turbulent flame speed.

In this paper we present experimental turbulent flame speed data measured in constant-pressure expanding flames, propagating in nearly homogenous isotropic turbulence for different values of Mk . Examining the data over a large range of conditions of pressure, u_{rms} and fuel: C_1 - C_4 hydrocarbons, we show that for all conditions, the scaling of Eq. (1) holds for a constant Mk . Furthermore, the normalized turbulent flame speed decreases with increasing Mk . Such a trend is in qualitative agreement with recent theoretical predictions [24].

2. Theory: Starting with the pioneering work of Kerstein *et al.* [3], the problem of premixed flame propagation in turbulent flows has often been analyzed using the G -equation. For the turbulent flame speed, the G -equation along with the flame surface density equation or the progress variable approach, namely the Bray-Moss-Libby model, have been used in the framework of Reynolds-Averaged Navier Stokes (RANS) equations formulation [4-6]. However, a RANS model with $k - \varepsilon$ type closure cannot consider the scale-dependent evolution of global properties. In general the multiscale nature of turbulence in premixed combustion has been considered only in very few analytical studies. In particular, Peters [25] proposed a spectral closure of the G -equation on the basis of dimensional arguments and extended it in [29] to include effects of gas expansion. A more rigorous but complex approach without thermal expansion was adopted by Collins and co-workers [30]-[31] by using the Eddy Damped Quasi Normal Markovian (EDQNM) approximation, which is one of the statistical closure theories for homogenous turbulence. All these approaches utilize the turbulent flame surface spectra with dissipation arising from flame properties such as Huygens propagation and positive Markstein length, $\delta_M = \delta_L Mk$.

It was recognized by Oberlack et al [33] that due to the generalized scaling symmetry of the G equation, Reynolds averaging of G cannot yield a unique mean flame position. This is due to the fact that the functional value of G on the interface, being a level set, does not carry any unique physical information. This problem could be circumvented, as in [24], for a statistically planar, steady flame with the mean direction of the surface normal chosen along the z -axis. A laminar flamelet is defined by its local laminar flame speed \tilde{S}_L where $\tilde{S}_L = S_L - S_L \delta_M \cdot \kappa - \delta_M \cdot S$; where S_L is the laminar flame speed of a planar premixed flame with respect to the unburnt gas; and κ and S are the local curvature and strain rate respectively. We define a z -distance function $g(x, y, z, t) = G(x, y, z, t) - z = G_N - z$ at all points $(x, y, z)_N$ belonging to each of the interfaces given by $G = G_N$ required for the field formulation. The flame can be considered to be one of these interfaces, say given by $G = G_0$. For the homogeneity and isotropy of the scalar field $g(x, y, z, t)$ over a volume, it is necessary that $\langle g(x, y, z, t) \rangle = 0$, obtained by averaging over each interface. This requires $\langle G \rangle = \langle z \rangle = G_N$ at each of the interfaces, constraining assignment of the level set values and suggesting once again that such a description is possible only for statistically planar and stationary interfaces in a homogenous isotropic fluctuating velocity field. A mean velocity in the z direction equal to the turbulent flame speed of the interfaces is required to ensure that each interface is statistically stationary. Of course, this also predefines the mean interface locations at $z = G_N$. However, defining g as the physical z -distance of the instantaneous interface position from the mean surface, Reynolds averaging and subsequent spectral closure by Peters [25] could be adopted for the g^2 transport equation as in [24]. As in any level set problem, the g^2 transport equation is defined within the entire cubic volume. Since the fluctuating velocity field is homogenous and isotropic and interfaces are planar and steady in the mean, we need not distinguish between the actual flame and other interfaces. As in the work by Kerstein *et al.* [3], volume averaging can be performed with ergodic hypothesis to yield global properties such as the surface area of the flame.

Following [25], the autocorrelation of the isotropic g field given by $R(\mathbf{r}, t) \equiv \langle g(\mathbf{x}, t)g(\mathbf{x} + \mathbf{r}, t) \rangle$ was Fourier transformed to yield the g^2 spectrum given by $\Gamma(k, t) = 4\pi k^2 \hat{R}(k, t)$, where \mathbf{r} is the separation vector, k the wavenumber and \hat{R} the Fourier

transform of R . The transport terms of the transport equation for $\Gamma(k, t)$, derived from the G equation, was closed by Pao's gradient transfer hypothesis and the dissipation terms were closed on the basis of dimensional arguments to give the following form of the g^2 spectrum.

$$\Gamma(k) = BH(k - k_I)k^{-5/3} \exp \left[-3c_1(2\pi)^{1/3} \left(\frac{U_{rms}}{S_L} \right)^{-1} \left(\frac{k}{k_I} \right)^{1/3} \right] \times \exp \left[-\frac{3}{4}(2\pi)^{4/3} c_2 Mk \left(\frac{U_{rms}}{S_L} \right)^{-1} \left(\frac{k_I}{k_L} \right) \left(\frac{k}{k_I} \right)^{4/3} \right] \quad (2)$$

where B is the integration constant and $H = H(k - k_I)$ is a function determined from initial conditions. Here H is chosen to be a Heaviside step function, *i.e.* $H = 0$ if $k < k_I$ and $H = 1$ otherwise, in such a manner that Γ is independent of time. Furthermore, c_1, c_2 are constants, $k_I = 2\pi / \lambda_I$, and $k_L = 2\pi / \delta_L$. In $\Gamma(k)$, the term $k^{-5/3}$ arises from stretching and wrinkling of the interfaces due to the imposed isotropic turbulence followed by two exponentially decaying dissipation terms. The first dissipation term is due to the nonlinear Huygens propagation or kinematic restoration. The second dissipation term is from the curvature dissipation by positive Mk . Peters [29] showed that including gas expansion effects, through the Sivashinsky integral, results in a term identical to the one due to kinematic restoration albeit with a positive sign within the exponent. Hence in strong turbulence, the net result of gas expansion is a reduction of dissipation by Huygens propagation, leaving the curvature dissipation term dominant. It is important to recognize that the expression of $\Gamma(k)$ given by Eq. (5) is only valid for positive Mk . Clearly a negative Mk would result in a blowup of the spectrum at large wavenumbers. While this mathematical difficulty precludes a rigorous analysis for negative Mk , the physics is still apparent in the spectrum, Eq. (2). It is well known that a negative Mk results in diffusion-thermal instability [23] manifested as amplification of flame surface fluctuations instead of dissipation (for positive Mk). The blowup of the spectrum for negative Mk thus indicates similar phenomena, though with the unrealistic unlimited amplification at high wavenumbers. However, it is known that even a negative Mk flame is only unstable at wavenumbers smaller than the flame thickness wavenumber as eventually thermal conduction will dominate to provide dissipation. This feature of higher wavenumber dissipation even for negative Mk is not captured by the current model and is left as a future work.

Kerstein *et al.* [3] showed that with the field formulation of the scalar g , the turbulent flame speed is given by the volume averaged functional of the absolute gradient of g for initially planar flames.

$$S_T / S_L = \langle |\nabla G| \rangle \approx \langle \sqrt{1 + \nabla g \cdot \nabla g} \rangle \quad (3)$$

To account for variation in laminar flame speed by stretch and curvature in the above normalization, it is possible to consider an average $\langle \tilde{S}_L \rangle = \langle S_L - S_L \delta_M \cdot \kappa - \delta_M \cdot S \rangle$. However, it has been shown experimentally that for large u_{rms} / S_L , curvature attains zero-centered symmetric distributions [34] -[35], thus resulting in $\langle \tilde{S}_L \rangle = S_L$. Even for statistically spherical expanding flames, the curvature distributions are found to be zero-centered and symmetric in strong turbulence [35] when a section of the flame is interrogated as discussed below. This suggests minimal influence of the global curvature due to sphericity of the flame in determining the turbulent flame speed, allowing extrapolation of statistically planar flame results to the expanding flame case. While the average laminar flame speed is unaffected due to equidistribution of curvature and strain rate, Mk alters local flame topology and thus global surface area by controlling dissipation of flame surface fluctuations.

It was shown in [24] that for the derivatives of g following normal distribution or the gradient squared of g following lognormal distribution, the following approximation holds, which allows determination of the turbulent flame speed directly from the spectrum given by Eq. (2),

$$S_T / S_L = \langle \sqrt{1 + \nabla g \cdot \nabla g} \rangle \approx \sqrt{\langle 1 + \nabla g \cdot \nabla g \rangle} = \sqrt{1 + \int_0^\infty k^2 \Gamma(k) dk} = \sqrt{1 + \int_{k_f}^\infty k^2 \Gamma(k) dk} \quad (4)$$

This was further simplified to finally yield the following scaling to the leading order:

$$\frac{S_T}{S_L} \sim \sqrt{\left(\frac{1}{Mk} \right) \left(\frac{U_{rms}}{S_L} \right) \left(\frac{\lambda_f}{\delta_L} \right)} \quad (5)$$

Thus from the result and discussion above, it is clear that the normalized turbulent flame speed should decrease with increasing Mk .

This result for the statistically planar flame could be extrapolated to a spherical configuration of interest in the present experiment, if the flame surface integral length

scale $\lambda \ll 2\pi\langle R \rangle$. Then a cube of the dimension λ could be selected to contain a statistically quasi-planar flame surface. This is elucidated in Fig. 1. The functional of the field variable g (Eq. 3) distributed over this cube could then be spatially integrated to give the normalized turbulent flame speed at each $\langle R \rangle$ location. Equation (5) obtained from the spectrum would yield the same result with λ_l being a linear function of $\langle R \rangle$ or replacing λ_l with simply $\langle R \rangle$ itself [36]. For unity- Le , methane-air flames at $\phi = 0.9$ [36], it was found that all the experimental data obtained over different u_{rms} and pressure could be scaled as $S_T / S_L \sim [(u_{rms} / S_L)(\langle R \rangle / \delta_L)]^{1/2}$.

3. Experiments: The experiments were conducted in a nearly constant-pressure apparatus that has been extensively employed in the study of laminar flames [37]. As shown in Fig. 2, the apparatus consists of an inner chamber situated within an outer chamber of much larger volume. The inner chamber consists of the cylindrical experimental test section (I.D. 4.5", O.D. 6.5", length 5"). The two ends of the chamber are sealed with 1" thick, 5" diameter, quartz windows which allow optical access. The inner chamber is filled with the test combustible gas while the outer chamber is filled with an inert gas of the same density. The two chambers can be opened to each other at the instant of spark ignition by rotating a sleeve that otherwise covers a matrix of holes connecting the two chambers, and the propagating flame is automatically quenched upon contacting the inert gas in the outer chamber. The flame propagation event is therefore basically isobaric because of the small volume of the inner chamber, hence preventing any perturbation by global pressure rise on the local flame structure. Another advantage of the design is that experiments can be conducted under high initial pressures, up to 60 bars as in the studies of Refs. [38]-[39], while preserving the integrity of the optical windows. Four fans of 2.7" diameter are located at its walls and are driven by motors enclosed in the outer chamber. Turbulence is generated by these orthogonally positioned fans as in [9] which continuously run during the entire flame propagation event. The fan-generated nonreacting turbulent flow field was characterized by high-speed particle image velocimetry (HS-PIV). Detailed flowfield statistics and quantification of the small but unavoidable deviation from isotropy could be found in [36]. The experiments were conducted at pressures of 1, 2, 3 and 5 bars and with u_{rms} at 1.34 and 2.85 m/s. The domain of experimentation was chosen to be $0.21 \leq \langle R \rangle / R_{chamber} \leq 0.38$, identified from

laminar flame speed experiments to avoid ignition and wall effects at the initial and final stages of flame propagation respectively.

4. Results: In this section we present normalized turbulent flame speed data from experiments performed with the following mixtures: C₂H₄-15%, O₂-85% N₂, $\phi=1.3$; C₂H₄-air, $\phi=1.3$; and n-C₄H₁₀-air, $\phi=0.8$. In addition, the CH₄-air, $\phi=0.9$ data from Ref [36] are also used for comparison purposes. All the relevant flame properties and the symbols that designate each condition of the experiment in subsequent figures are given in Table. 1. The values of Mk for all conditions were obtained from laminar expanding flame experiments using the methodologies detailed in [39]. The turbulent flame speed data are extracted from the time derivative of the average radius: $d\langle R \rangle / dt$, where $\langle R \rangle$ is defined as $\langle R \rangle = \sqrt{A/\pi}$, A is the area enclosed by the flame edge tracked from the high-speed Schlieren imaging. It is important to recognize that $d\langle R \rangle / dt \neq S_T^b$ due to gas expansion effects. As suggested in Ref [19] the normalized turbulent flame speed can be defined as the mean propagation rate of the $\langle c \rangle = 0.5$ iso-surface and can be extracted from $d\langle R \rangle / dt$, obtained from Schlieren imaging as the following:

$$S_T / S_L = (2\Theta / (\Theta + 1)) (r_0^2 / r_{0.5}^2) (S_L^b)^{-1} (d\langle R \rangle / dt) \quad (6)$$

The normalized turbulent flame speeds for pressure varying from 1 to 5atms and at u_{rms} of 1.43 and 2.85m/s are presented in Fig. 3. Clearly each set of data corresponding to a particular mixture collapses reasonably well on a single straight line, suggesting the general validity of the $S_T / S_L \sim [(u_{rms} / S_L) (\langle R \rangle / \delta_L)]^{1/2}$ scaling irrespective of the fuel-air mixtures. Of course for different mixtures the data sets collapse on different lines indicating the influence of Mk . As shown in Table 1 for a given mixture such as CH₄-air, $\phi=0.9$, the variation in Mk over pressure is small; hence including Mk in the scaling above will not result in any discernable deviation of the data from a single line for a given mixture. The variation of Mk over different mixtures is however significant. While the C₂H₄-air, $\phi=1.3$ mixture has a positive Mk , reduction of O₂ concentration to 15% results in a negative Mk due to the significant reduction in the thermal expansion. As shown in Fig. 3 the S_T / S_L for the C₂H₄ mixtures (15% O₂, 85% N₂, $\phi=1.3$) corresponding to negative Mk , are the highest, followed by the S_T / S_L for the CH₄-air mixtures with $\phi=0.9$, corresponding to an Mk near unity. The S_T / S_L for the C₂H₄-air mixtures with

$\phi=1.3$ is next in terms of magnitudes with Mk between 1.4 to 2.0. The lowest S_T/S_L is observed for the n-C₄H₁₀-air mixtures with $\phi=0.8$, which has the highest $Mk = 2.8$ among all the mixtures studied. This last set of data shows some scatter possibly caused by local extinction in strong turbulence, due to strong non-equidiffusive effects.

Summarizing, using C₁, C₂ and C₄ hydrocarbon fuels we have shown the following: (a) the scaling of $S_T/S_L = \left[(U_{rms}/S_L) \left((R)/\delta_L \right) \right]^{0.5} = \text{Re}_{T,f}^{0.5}$ is valid for these C₁-C₄ hydrocarbons, (b) for a constant $\text{Re}_{T,f}$, S_T/S_L decreases with increasing Mk . This trend is also predicted by the theoretical result of Eq. (5) although with the restriction of positive Mk . (c) Therefore, from (a) and (b) a further degree of validation of the theoretical results beyond the general scaling is provided. Such a trend was also experimentally observed by Fairweather *et al.* [42] as they measured S_T/S_L over different equivalence ratios of CH₄-air flames along with H₂ addition. The observation, however, was empirical and the evolutionary nature of S_T/S_L due to the scale dependence was not considered. In the present work, we have utilized the well-known concept of modification of laminar flame speed due to curvature by Mk , to couple with the statistical turbulence theory to arrive at an expression for normalized S_T/S_L . However, unlike an expanding laminar flame which has only one length scale and curvature, an expanding turbulent flame has a spectrum of length scales and curvatures due to wrinkling by the flow turbulence. The propagation rate of an expanding laminar flame is therefore modified by Mk through the single curvature, whereas for a turbulent flame the cumulative effect of Mk on the overall distribution of curvatures modifies the normalized turbulent flame speed. This cumulative effect, from the largest to the smallest length scales controlled by the Mk is the fundamental cause behind emergence of these two limiting length scales in the scaling relationship used for collapsing the data in Fig. 3.

To show that the proposed scaling and Mk dependence is independent of burner geometry, we extract the relevant data (moderate to large Reynolds number and for the Mk specified cases) for H₂-CO-air mixtures, from a recent work by Venkateswaran *et al.* for burners of different sizes [43] and present it in the framework of the proposed scaling in Fig. 4. Clearly the data for the larger Mk cases collapses reasonably well on single straight lines, once again suggesting the validity of the scaling given by (1). For strongly negative Mk , obtained by increasing the H₂ concentration, there are small deviations from linearity which can be attributed

to the additional influence by diffusional-thermal instability. But more importantly, the same effect of reduced S_T/S_L with increasing Mk is clearly observed and thus validated across different burner geometries.

5. Conclusions: We have presented experimental results of turbulent flame speeds for CH₄, C₂H₄, and n-C₄H₁₀-air mixtures and have shown that irrespective of the fuel, the normalized turbulent flame speed data follows the recent theoretical and experimental $Re_{T,f}^{0.5}$ scaling, in which the average radius is the length scale and thermal diffusivity is the transport property. For a constant $Re_{T,f}$, it is experimentally observed that the normalized turbulent flame speed decreases with increasing Mk which can be theoretically explained as a cumulative effect of increased dissipation of the flame surface curvature from the largest to the smallest length scales.

Acknowledgements:

This work was supported by the Combustion Energy Frontier Research Center, an Energy Frontier Research Center funded by the U.S. Department of Energy, Office of Basic Energy Sciences under Award Number DE-SC0001198 and by the Air Force Office of Scientific Research.

References

- [1] P. Clavin, F. A. Williams, *Journal of Fluid Mechanics* 90 (1979) 589.
- [2] V. Yakhot, *Combustion Science and Technology* 60 (1988) 191.
- [3] A. R. Kerstein, W. T. Ashurst, F. A. Williams, *Physical Review A* 37 (1988) 2728.
- [4] A. R. Kerstein, W. T. Ashurst, *Physical Review Letters* 68 (1992) 934.
- [5] A. Pocheau, *Physical Review E* 49 (1994) 1109.
- [6] B. Denet, *Physical Review E* 55 (1997) 6911.
- [7] N. Peters, *Journal of Fluid Mechanics* 384 (1999) 107.
- [8] H. Kolla, N. Rogerson, N. Swaminathan, *Combustion Science & Technology* 182 (2010) 284.
- [9] R.G. Abdel-Gayed, D. Bradley, M. Lawes, *Proc. Roy. Soc. Lond. A* 414 (1987) 389

- [10] D. Bradley, C. G. W. Sheppard, R. Woolley, D. A. Greenhalgh, R. D. Lockett, *Combustion and Flame* 122 (2000) 195.
- [11] D. Bradley, M. Lawes, M.S. Mansour, *Combustion and Flame* 158 (2011) 123
- [12] S. A. Filatyev, J. F. Driscoll, C. D. Carter, J. M. Donbar, *Combustion and Flame* 141 (2005) 1
- [13] S. Kwon, M.S. Wu, J.F. Driscoll, G.M. Faeth, *Combustion and Flame* 88, 2 (1992) 221
- [14] Kobayashi, T. Tamura, K. Maruta, T. Niioka, *Proceedings of the Combustion Institute* 26 (1996) 389.
- [15] H. Kobayashi, K. Seyama, H. Hagiwara, Y. Ogami, *Proceedings of the Combustion Institute* 30 (2005) 827.
- [16] J.B. Bell, M.S. Day, I.G. Shepherd, M.R. Johnson, R.K. Cheng, J.F. Grcar, et al. *Proceedings of the National Academy of Sciences* 2005;102(29):10006–11.
- [17] Y. Shim, S. Tanaka, M. Tanahashi, T. Miyauchi, *Proceedings of the Combustion Institute* 33 (2010) 1455.
- [18] N. Peters, *Turbulent Combustion*, Cambridge University Press, NY, 2000.
- [19] J. F. Driscoll, *Progress in Energy & Combustion Science* 34 (2008) 91.
- [20] A. N. Lipatnikov, J. Chomiak, *Progress in Energy & Combustion Science* 36 (2010) 1.
- [21] A. N. Lipatnikov, J. Chomiak, *Progress in Energy & Combustion Science* 28 (2002) 1.
- [22] S.B. Pope, *Annual Review of Fluid Mechanics*, 19 (1987), 237
- [23] C. K. Law, *Combustion Physics*, Cambridge University Press, NY, 2006.
- [24] S. Chaudhuri, V. Akkerman, C.K. Law, *Physical Review E*, 84, (2011) 026322.
- [25] N. Peters, *Journal of Fluid Mechanics* 242 (1992) 611.
- [26] N. Peters, *Journal of Fluid Mechanics* 384 (1999) 107.
- [27] N. Swaminathan, K. N. C. Bray, *Combustion & Flame* 143 (2005) 549.
- [28] H. Kolla, N. Rogerson, N. Swaminathan, *Combustion Science & Technology* 182 (2010) 284.
- [29] N. Peters, H. Wenzel, F. A. Williams, *Proceedings of the Combustion Institute* 28 (2000) 235.
- [30] A. Dandekar, L. Collins, *Combustion & Flame* 101 (1995) 428.
- [31] L. Collins, M. Ultisky, *Proceedings of the Combustion Institute* 26 (1996) 315.
- [32] L. R. Collins, *Computers and Fluids* 24 (1995) 663.

- [33] M. Oberlack, H. Wenzel, N. Peters, *Combustion Theory and Modelling*, 5 (2001) 363-383.
- [34] I. G. Shepherd, R. K. Cheng, T. Plessing, C. Kortschik and N. Peters, *Proceedings of the Combustion Institute* 29 (2002) 1833.
- [35] M.Z. Haq, C.G.W Sheppard, R Woolley, D.A Greenhalgh, R.D Lockett, *Combustion and Flame*, 131 (2002) 1-15.
- [36] S. Chaudhuri, F. Wu, D. Zhu, C.K. Law, *Physical Review Letters*, 108, (2012), 044503
- [37] S. D. Tse, D. L. Zhu, C. K. Law, *Review of Scientific Instruments*, 75, 1, (2004), 233
- [38] G. Rozenchan, D.L. Zhu, C.K. Law, *Proceedings of the Combustion Institute*, 29, (2002) 1461
- [39] A. P. Kelley and C. K. Law, *Combustion and Flame*, 156, 6, (2009) 1844.
- [40] R. J. Kee, F. M. Rupley, J. A. Miller, et al., CHEMKIN Collection, Release 3.6, 2000.
- [41] H. Wang, X.Q. You, A.V. Joshi, S.G. Davis, A. Laskin, F. Egolfopoulos, C.K. Law, USC Mech Version II. High-Temperature Combustion Reaction Model of H₂/CO/C₁-C₄ Compounds, May 2007. <http://ignis.usc.edu/USC_Mech_II.htm>.
- [42] M. Fairweather, M.P. Ormsby, C.G.W. Sheppard, R. Woolley, *Combustion and Flame*, 156 (2009) 780.
- [43] P. Venkateswaran, A. Marshall, D. H. Shin, D. Noble, J. Seitzman, T. Lieuwen, *Combustion and Flame*, 158 (2011) 1602.

TABLE AND FIGURE CAPTIONS:

Table 1: Legends, laminar flame properties and turbulent intensity for all experimental conditions.

Figure 1: Schematic of the statistically quasi planar assumption for an expanding flame to utilize the theoretical scaling of Eq. (5). The shaded squares are the vertical cross sections of cubes of dimension λ_i .

Figure 2: Schematic of experimental setup showing the dual chamber apparatus.

Figure 3: Normalized turbulent flame speed versus $\sqrt{(U_{rms}/S_L)(\langle R \rangle/\delta_L)} = \text{Re}_{T,f}^{0.5}$ for C₂H₄-15% O₂- 85% N₂, $\phi=1.3$; C₂H₄-air, $\phi=1.3$ and n-C₄H₁₀-air, $\phi=0.8$ mixtures. The symbols for each experimental condition and corresponding laminar flame and turbulence parameters could be found in Table 1.

Figure 4: Normalized turbulent flame speed versus $\sqrt{(U_{rms}/S_L)(L/\delta_L)} = \text{Re}_{T,f}^{0.5}$ for Bunsen flames of different burner sizes. The data is extracted from Venkateswaran et al. [43].

FIGURES AND TABLES:

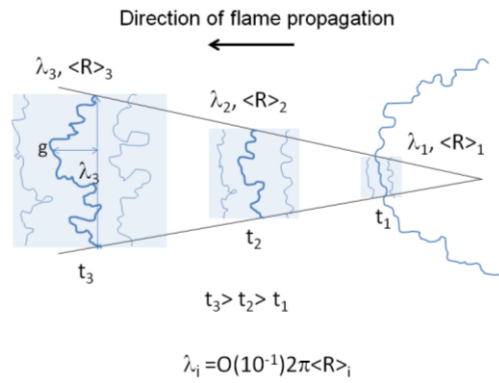
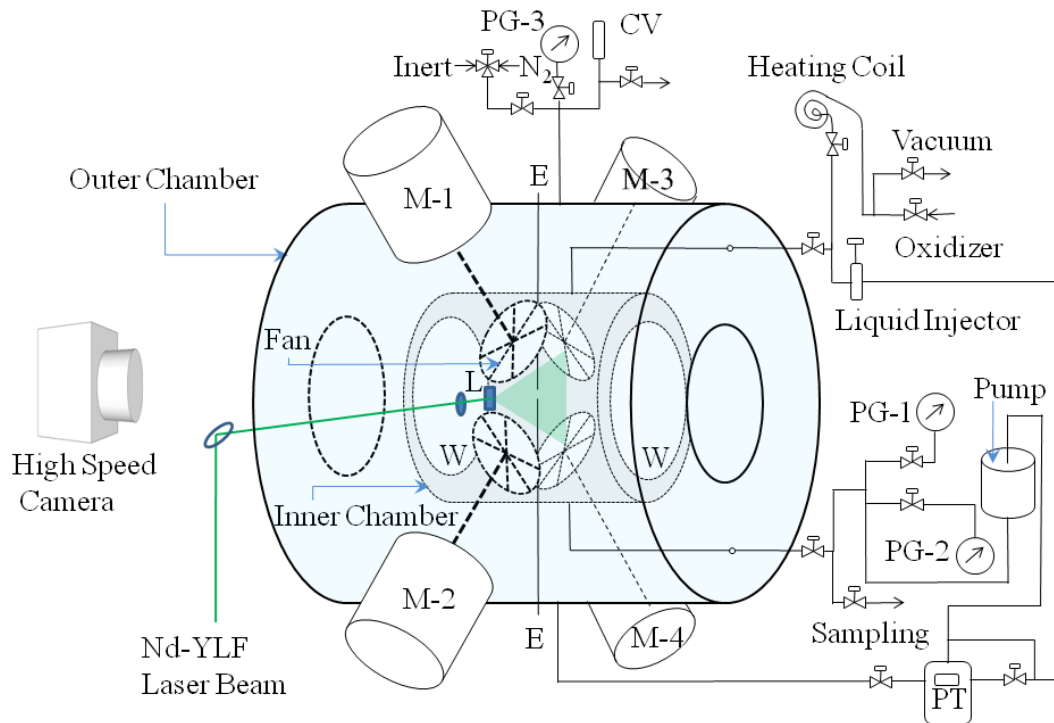


Figure 1: Schematic of the statistically quasi planar assumption for an expanding flame to utilize the theoretical scaling of Eq. (5). The shaded squares are the vertical cross sections of cubes of dimension λ_i .



CV: Check Valve, PG: Pressure Gauge, PT: Pressure Transducer, M: Fan Motor, L: Cylindrical Lens, E: Electrodes, W: Quartz Window

Figure 2: Schematic of experimental setup showing the dual chamber apparatus.

Symbol	Mixture	ϕ	p/p_0	rpm	u_{rms} (m/s)	S_L (m/s) ¹	$S_{L,b}$ (m/s) ¹	δ_L (m) ¹	Mk ²
	CH ₄ -air	0.9	1	2000	1.43	0.32	2.31	4.80E-04	1.03
	CH ₄ -air	0.9	1	4000	2.85	0.32	2.31	4.80E-04	1.03
	CH ₄ -air	0.9	2	4000	2.85	0.25	1.83	2.90E-04	
	CH ₄ -air	0.9	3	4000	2.85	0.22	1.57	2.20E-04	
	CH ₄ -air	0.9	5	2000	1.43	0.17	1.28	1.60E-04	0.75
	CH ₄ -air	0.9	5	4000	2.85	0.17	1.28	1.60E-04	0.75
	C ₂ H ₄ -15% O ₂ -85% N ₂	1.3	2	2000	1.43	0.18	1.15	3.67E-04	
	C ₂ H ₄ -15% O ₂ -85% N ₂	1.3	2	4000	2.85	0.18	1.15	3.67E-04	
	C ₂ H ₄ -15% O ₂ -85% N ₂	1.3	5	2000	1.43	0.11	0.75	2.17E-04	-1.10
	C ₂ H ₄ -15% O ₂ -85% N ₂	1.3	5	4000	2.85	0.11	0.75	2.17E-04	-1.10
	C ₂ H ₄ -air	1.3	1	2000	1.43	0.61	5.01	2.92E-04	1.44
	C ₂ H ₄ -air	1.3	1	4000	2.85	0.61	5.01	2.92E-04	1.44
	C ₂ H ₄ -air	1.3	3	2000	1.43	0.48	3.95	1.16E-04	
	C ₂ H ₄ -air	1.3	5	4000	2.85	0.41	3.42	7.85E-05	2.03
	n-C ₄ H ₁₀ -air	0.8	5	4000	2.85	0.18	1.18	1.18E-02	2.75

¹ Computed with PREMIX in Chemkin II with USC Mech II , Refs [40-41]

² Data from new and past laminar flame speed experiments

Table 1: Legends, laminar flame properties and turbulent intensity for all experimental conditions.

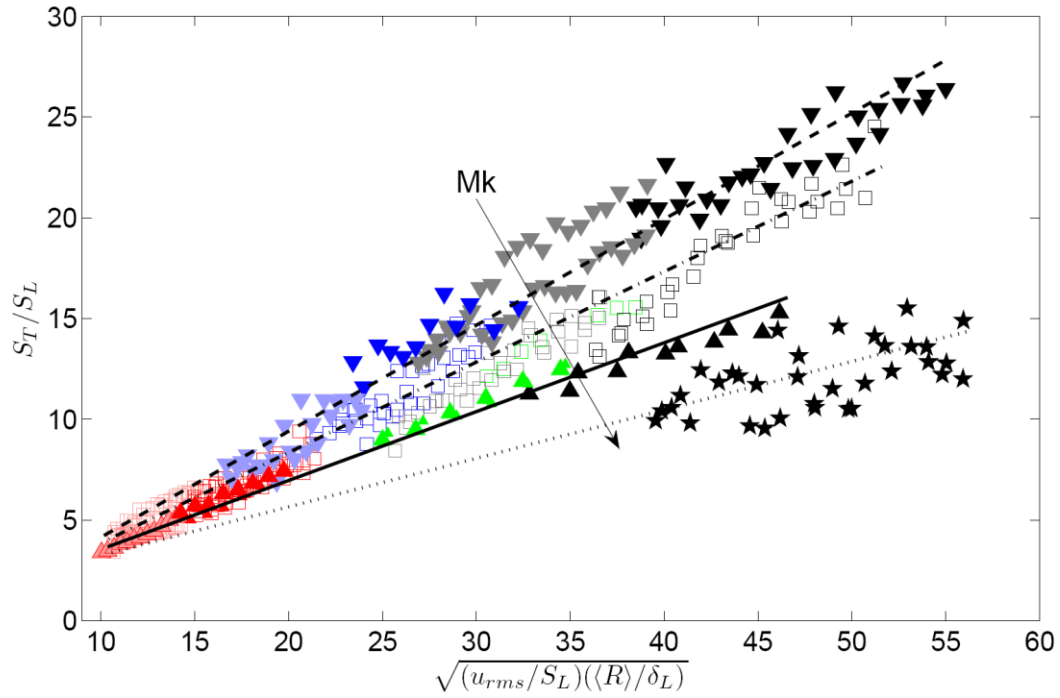


Figure 3: Normalized turbulent flame speed versus $\sqrt{(U_{rms}/S_L)((R)/\delta_L)} = \text{Re}_{T,f}^{0.5}$ for C_2H_4 -15% O_2 - 85% N_2 , $\phi=1.3$; C_2H_4 -air, $\phi=1.3$ and n- C_4H_{10} -air, $\phi=0.8$ mixtures. The symbols for each experimental condition and corresponding laminar flame and turbulence parameters could be found in Table 1.

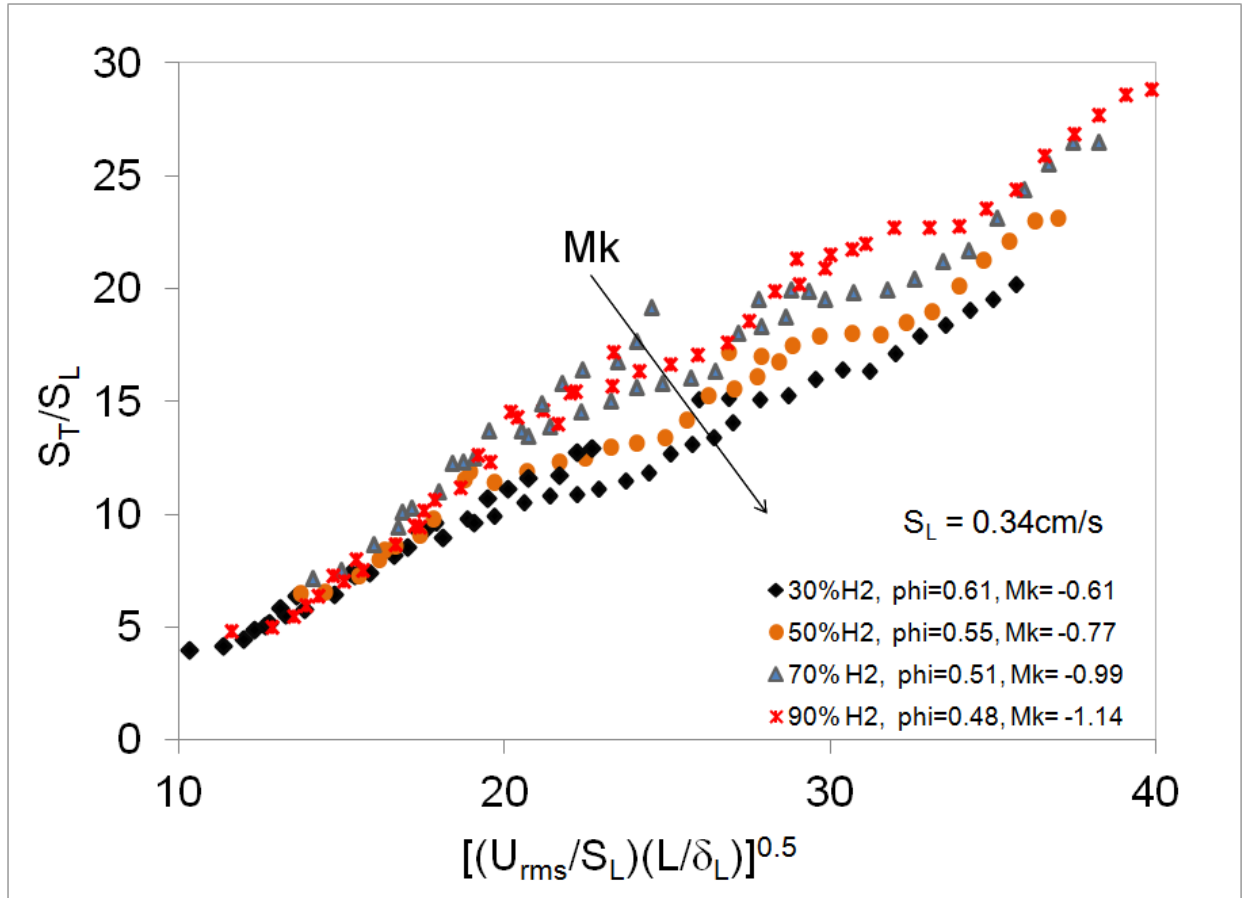


Figure 4: Normalized turbulent flame speed versus $\sqrt{(U_{rms}/S_L)(L/\delta_L)} = \text{Re}_{T,f}^{0.5}$ for Bunsen flames of different burner sizes. The data is extracted from Venkateswaran et al. [43].